

# Electric-field-induced superconductivity in electrochemically etched ultrathin FeSe films on SrTiO<sub>3</sub> and MgO

J. Shiogai<sup>1\*</sup>, Y. Ito<sup>1</sup>, T. Mitsuhashi<sup>1</sup>, T. Nojima<sup>1</sup> and A. Tsukazaki<sup>1,2</sup>

**Among the recently discovered iron-based superconductors<sup>1–3</sup>, ultrathin films of FeSe grown on SrTiO<sub>3</sub> substrates have uniquely evolved into a high-transition-temperature ( $T_c$ ) superconducting material<sup>4–15</sup>. The mechanisms for the high- $T_c$  superconductivity are under debate, with the superconducting gap mainly characterized with *in situ* analysis for FeSe films grown by molecular beam epitaxy. Here, we investigate the high- $T_c$  superconductivity in ultrathin FeSe using an alternative top-down electrochemical etching technique in a three-terminal transistor configuration. In addition to the high-temperature superconductivity in FeSe on SrTiO<sub>3</sub>, the electrochemically etched ultrathin FeSe transistor on MgO also exhibits superconductivity around 40 K, implying that the application of an electric field effectively contributes to the high- $T_c$  superconductivity in ultrathin FeSe regardless of substrate material. Moreover, the observable critical thickness for the high- $T_c$  superconductivity is expanded up to 10 unit cells under an applied electric field and the insulator–superconductor transition is electrostatically controlled. The present demonstration implies that the modification of charge imbalance of holes and electrons by the electric-field effect plays a crucial role in inducing high- $T_c$  superconductivity in FeSe-based electric double-layer transistors.**

Iron selenide (FeSe) is one of a family of iron-based superconductors ( $T_c \sim 8$  K; refs 1–3), having a tetragonal PbO structure consisting of the layered atomic stacking of iron and selenium along the  $c$ -axis. In single or two unit-cell-thick FeSe films grown by state-of-the-art bottom-up molecular beam epitaxy (MBE; refs 4–15) on insulating SrTiO<sub>3</sub> (refs 12–14) or Nb-doped SrTiO<sub>3</sub> (refs 4–12,15), a large superconducting gap of about 20 meV has been detected by angle-resolved photoemission spectroscopy (ARPES; refs 4–10) and scanning tunnelling microscopy (STM; ref. 11). Compared to expected  $T_c$  values as high as 65 K (ref. 6) or 80 K (ref. 11) from the large gap energy evaluated by ARPES or STM, the temperature dependence of resistivity yields a consensus of the onset  $T_c$  value about 40 K (refs 11–14). However, a very recent report of superconductivity above 100 K detected by *in situ* electrical resistance measurements for FeSe films grown on Nb-doped SrTiO<sub>3</sub> would apparently increase the spread in  $T_c$  (refs 15,16). The mechanisms for the enhancement of the superconducting gap energy in ultrathin FeSe are now considered to be strong electron–phonon coupling<sup>10</sup>, variation of the electronic band structure at the M point and the  $\Gamma$  point<sup>4</sup>, and a charge transfer effect from the substrates<sup>5,13,17</sup>. *Ex situ* characterizations based on the temperature dependence of resistivity regarding the effect of an electric field, magnetic field, thickness

dependence of  $T_c$  and substrate material dependence are matters of interest for a deeper understanding of high- $T_c$  superconductivity in ultrathin FeSe studies.

In contrast to the *in situ* bottom-up MBE technique, classical electrochemical etching is one of the best means of carrying out a top-down approach to ultrathin FeSe films, owing to a high uniformity and fine tunability in thickness being possible through continuous monitoring of the electrical current originating from the electrochemical reaction. In our experiments, we employed this electrochemical etching approach in a three-terminal transistor configuration, the so-called electric double-layer (EDL) transistor (Fig. 1a)<sup>18</sup>. The EDL transistors were fabricated from 13- and 18-nm-thick FeSe films grown on insulating SrTiO<sub>3</sub> and MgO substrates, respectively, by pulsed-laser deposition, as described in Methods. The films and Pt gate electrode are covered with the ionic liquid (IL) *N,N*-dethyl-*N*-methyl-*N*-(2-methoxyethyl)ammonium bis(trifluoromethanesulphonyl)imide (DEME-TFSI), as schematically shown in Fig. 1a. The original concept of the EDL transistor involves an electrostatic charge carrier doping based on the giant capacitance originating from a very narrow (<1 nm) EDL width. Following this concept, various kinds of physical phenomena, such as superconductivity<sup>18–23</sup>, ferromagnetism<sup>24</sup> and an insulator–metal transition in correlated electron systems<sup>25</sup>, have been induced or controlled electrostatically. Another feature of EDL transistors is the electrochemical reaction<sup>26–28</sup>. These two features appear separately, with some boundary that depends on the temperature of the IL and the applied gate voltage<sup>26,27</sup>, as schematically shown by the dashed black line in Fig. 1b. In this study, we have applied an electrostatic doping effect with varying  $V_G$  below the characteristic temperature (blue arrow in Fig. 1b) and electrochemical etching to peel FeSe layers while tuning the sample temperature under a constant applied  $V_G$  (red arrow in Fig. 1b). For each etching sequence, the systematic dependence on thickness and the effect of the field on superconductivity in FeSe films can be investigated, all within a single EDL transistor.

The temperature dependence of the channel sheet resistance ( $R_s$ – $T$  curve) and its superconducting properties were measured using a standard d.c. four-terminal method. In the initial thick films on SrTiO<sub>3</sub> and on MgO, onset superconducting transition temperatures  $T_c^{\text{on}} = 8.2$  K and 4.8 K are clearly observed on lowering the temperature  $T$ , as shown in Fig. 1c (solid lines), which is consistent with the bulk properties of FeSe (ref. 3). No significant change in the  $R_s$ – $T$  curves (broken lines) is observed with electrostatic doping using  $V_G = 5$  V at 220 K for the initial thick condition, implying that

<sup>1</sup>Institute for Materials Research, Tohoku University, Sendai 980-8577, Japan. <sup>2</sup>PRESTO, Japan Science and Technology Agency (JST), Chiyoda-ku, Tokyo 102-0075, Japan. \*e-mail: junichi.shiogai@imr.tohoku.ac.jp

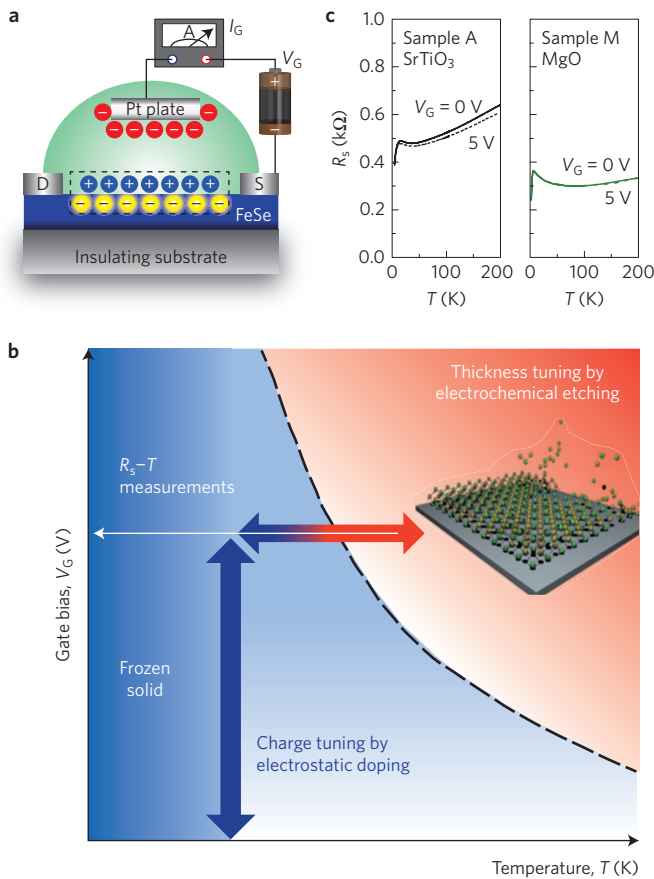


**Figure 1 | Electrochemical etching and electrostatic doping in the electric double-layer transistor.** **a**, Schematic of the EDL transistor composed of FeSe films on insulating SrTiO<sub>3</sub> and MgO substrates. The side gate voltage  $V_G$  is applied through the ionic liquid. The gate leakage current  $I_G$  is measured using a picoammeter, which is a measure for the degree of etching. **b**, Schematic illustrating the operation of an EDL transistor as a function of  $V_G$  and temperature  $T$ . The broken line indicates the boundary between electrostatic doping and electrochemical etching. **c**,  $R_s$ - $T$  curves of sample A on SrTiO<sub>3</sub> and sample M on MgO for the initial thick condition when  $V_G = 0$  V (solid lines) and 5 V (broken lines) are applied.

high- $T_c$  superconductivity is not induced at the IL/FeSe interface (see Supplementary Information) at this temperature.

The high- $T_c$  superconductivity appears in FeSe films grown on both SrTiO<sub>3</sub> (sample A) and MgO (sample N) after a series of etching, as shown in Fig. 2a,b. During the etching sequence, with a constant  $V_G = 5$  V at about 245 K,  $R_s$ - $T$  measurements were performed regularly (black arrow in Fig. 1b) showing that the onset  $T_c$  in the normalized sheet resistance  $R_s/R_s^{100K}$  is greatly increased from the bulk value up to  $T_c^{on} = 43.3$  and 39.0 K for samples A and N, respectively (the corresponding raw data are presented in Supplementary Information). The estimated  $T_c^{on}$  values from  $R_s$ - $T$  curves shown in Fig. 2a,b are summarized in Fig. 2c,d as a function of the average thickness, which is carefully estimated from the initial thickness and the etching rate in the electrochemical reaction from the gate leakage current (see Supplementary Information). There are four implications derived from these figures. The first implication is that two-step transitions are observed in the intermediate etching region. Accompanying the enhancement of metallic behaviour,  $R_s$  drops first at around  $T = 30$  K, with second steps at 8 K and 4 K in the case of FeSe on SrTiO<sub>3</sub> and MgO, respectively, giving a first signature of the appearance of high- $T_c$  superconducting region in the device. The systematic disappearance of the bulky low- $T_c$  region with decreasing thickness is evidence of our fine

tuning of the thicknesses. Indeed, the zero-resistance temperature of about 30 K implies that the FeSe layers are uniformly etched down to approximately one/two unit cells in thickness in our primitive devices. The second implication is that the high- $T_c$  superconductivity emerges in the ultrathin FeSe film on MgO as a result of the electric-field effect in the EDL transistor. Such high- $T_c$  superconductivity in FeSe on MgO has not been reported in *in situ* MBE studies—probably owing to there being no charge transfer from MgO to FeSe. In reality, in Hall effect measurements on high- $T_c$  one/two-unit-cell-thick FeSe on MgO, a negative Hall coefficient is observed, indicating electron accumulation is realized. The third implication is that the values of  $T_c^{on}$  for both samples on SrTiO<sub>3</sub> and MgO are close to the highest values that have been reported in capped single-unit-cell-thick FeSe films grown by MBE (refs 12–14). If the disorder at the IL/FeSe interface limits  $T_c$  to about 40 K, as low as the capped FeSe, further improvements of the interface quality are required to enhance  $T_c^{on}$  towards 100 K (refs 15,16). The final implication is that the high- $T_c$  superconductivity emerges under a relatively thicker condition of about ten unit cells, followed by a weak thickness dependence. At present, it is not clear whether the whole thick-film region contributes high- $T_c$  superconductivity or not. We will return to this later.

To further investigate the superconducting properties, we performed  $R_s$ - $T$  measurements under perpendicular magnetic fields  $B$  for sample N on MgO. As shown in Fig. 2e, the tail of the resistive transition is broadened by applying  $B$ , indicating the two-dimensional nature of the FeSe film. Figure 2f shows the temperature dependence of the perpendicular upper critical field  $B_{c2}(T)$  derived from the midpoint temperature of the resistance drop  $T_c(B)$  in the  $R_s$ - $T$  curves in Fig. 2e. From the linear relation, which is consistent with the Ginzburg–Landau (GL) theory given as  $B_{c2}(T) = (\phi_0/(2\pi\xi^2(0)))(1 - (T/T_c(0)))$ , with  $\phi_0$  and  $\xi(0)$  being the flux quantum and the GL coherence length at zero temperature, respectively, we obtained  $\xi(0) = 2.0$  nm, which is around half of the bulk value<sup>3</sup>. We further compare the GL coherence length  $\xi(0)$  to the expression of  $0.74\xi_0$  in the clean limit based on the Bardeen, Cooper, and Schrieffer (BCS) theory with  $\xi_0 = \hbar v_F/\pi\Delta(0) = \hbar v_F/\pi(1.76k_B T_c)$ . Here,  $\hbar$ ,  $v_F$ ,  $\Delta(0)$  and  $k_B$  are the reduced Planck constant, Fermi velocity, BCS superconducting gap and Boltzmann constant, respectively. Using a value of  $v_F \sim 9.56 \times 10^4$  m s<sup>-1</sup> (ref. 5), we determined  $0.74\xi_0$  to be  $\sim 2.1$  nm. This value is comparable to  $\xi(0) = 2.0$  nm obtained from the experiments, indicating the system is almost in the clean limit.

Returning to the thickness dependence of  $T_c^{on}$  in Fig. 2c,d, we note that the first single-step superconducting transition occurs at thicknesses of 9.6 nm and 5.9 nm for samples A and N, respectively. The appearance of high- $T_c$  superconductivity in the rather thicker conditions prompted us to consider how the electric-field effect contributes. Here, we examined the effect of electrostatic doping on the superconductivity in both ultrathin and thicker conditions using different experimental schemes in the same device set-up as for sample A. First, samples B and C on SrTiO<sub>3</sub>, and samples M and L on MgO were etched at  $T = 245$  K to induce the superconductivity, as shown in Fig. 3a, the top panel of Fig. 3c, and in Fig. 3d (red line data) and the inset of Fig. 3d (red line data). The thicknesses of sample B on SrTiO<sub>3</sub> and sample L on MgO are tuned to approximately one/two unit cells in thickness (the red square in Fig. 2c and the purple triangle in Fig. 2d), whereas sample C on SrTiO<sub>3</sub> and sample M on MgO are etched to intermediate thicknesses of 9.4 nm (the blue triangle in Fig. 2c) and 3.7 nm (the green circle in Fig. 2d), by monitoring the leakage current under the assumption that the same etching rate holds as for sample A. After detection of the high- $T_c$  superconducting behaviour, we examined the electrostatic effect by removing and then reapplying  $V_G$  at  $T = 220$  K (along the blue arrow in Fig. 1b; note that no electrochemical etching occurs at this temperature, as mentioned above).

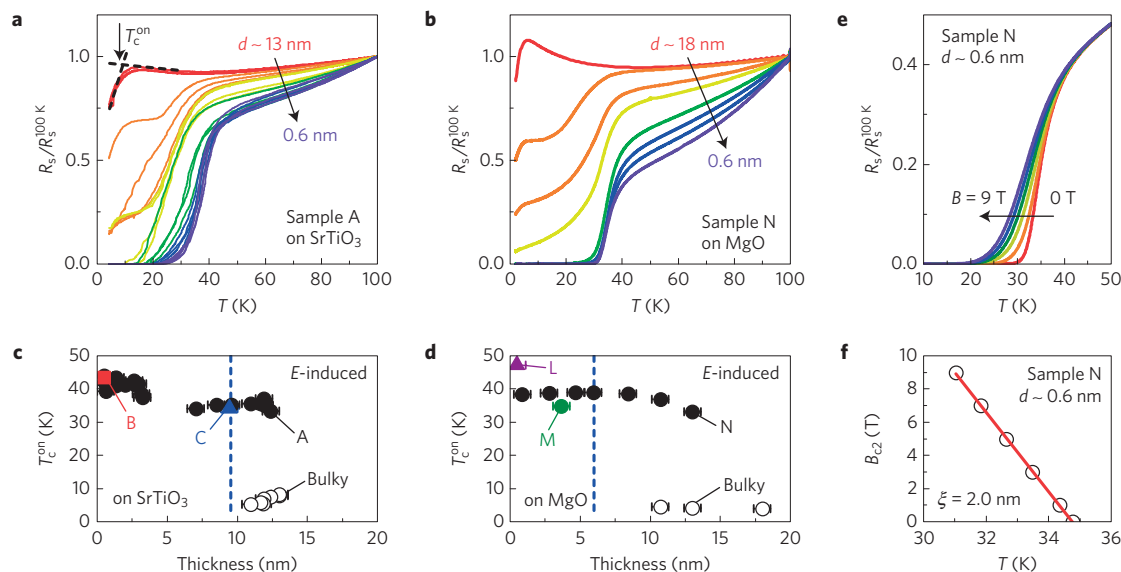


**Figure 2 | Thickness tuning of FeSe on SrTiO<sub>3</sub> and MgO via electrochemical etching.** **a, b**, Sheet resistance normalized to the value at  $T=100$  K,  $R_s/R_s^{100\text{K}}$ , as a function of temperature  $T$  for continuing etching processes—that is, different film thickness ( $d$ )—for sample A on SrTiO<sub>3</sub> (**a**) and for sample N on MgO (**b**). (For the detailed information on the thickness, see Supplementary Information.) The onset superconducting transition temperature  $T_c^{\text{on}}$  is defined by the intersection of the two dashed linear extrapolation lines. **c, d**,  $T_c^{\text{on}}$  for samples A and N shown in **a, b** are collected as a function of averaged thickness for the electric-field-induced high- $T_c$  ( $E$ -induced; filled black circles) and the initial bulk-like low- $T_c$  (open black circles) conditions. A vertical broken line corresponds to the thickness for the first data showing a single-step transition in the  $R_s$ - $T$  curves. The data for samples B, C, M and L after etching and at  $V_G=5$  V are indicated by red square, blue triangle, green circle and purple triangle, respectively. Vertical error bars of 0.6 nm, corresponding to 1 u.c. of FeSe, are determined by the surface roughness of as-grown film measured by atomic force microscopy (see Supplementary Information). **e**, Perpendicular magnetic field dependence of  $R_s$ - $T$  curves of sample N after etching down to approximately one/two unit cells in thickness measured at  $B=0$  T (red), 1 T (orange), 3 T (yellow), 5 T (green), 7 T (blue) and 9 T (purple). **f**, Temperature dependence of the upper critical field  $B_{c2}$  (T) derived from the midpoint of the resistance drop in **e**. The red line corresponds to a linear fitting line based on the GL theory.

For sample B, expectedly at a thickness of one/two unit cells, the initial insulating behaviour was not recovered on reducing  $V_G$  from 5 to 3 and then to 0 V, as shown in Fig. 3b. This result is good evidence for the thickness having reached close to one/two unit cells, because the high- $T_c$  superconductivity under  $V_G=0$  V is consistent with the result of a previous report on FeSe/SrTiO<sub>3</sub> with charge transfer solely from the SrTiO<sub>3</sub> substrate<sup>13</sup>. Interestingly, the increase of  $T_c^{\text{on}}$  from 43.5 to 46.3 K as a result of reduced  $V_G$  implicates an over-doping effect from electrostatic doping. In contrast, in sample C, under the thicker 9.4 nm condition, the superconductivity vanishes and the  $R_s$ - $T$  curve returns to insulating behaviour when  $V_G$  is removed (blue line in middle panel of Fig. 3c). The reappearance of insulating behaviour indicates uniform etching without a local ultrathin region providing a high- $T_c$  superconducting current path. Then, application of  $V_G=5$  V recovers the superconductivity (blue line in bottom panel of Fig. 3c), demonstrating reversible control of the insulator–superconductor transition by electrostatic means. We note that the possibility of intercalation can be excluded for two reasons: no significant variation of the  $c$ -axis length was observed after etching (see Supplementary Information) and reversible control of the insulator–superconductor transition was possible by gating. This series of results in sample C suggests that the observable thickness condition for high- $T_c^{\text{on}}$  superconductivity is greatly expanded from one/two unit cells to more than ten unit cells by the application of an electric field. Furthermore,  $T_c^{\text{on}}$  values in samples M and L decrease on reducing the accumulated charge, as shown in Fig. 3d. Therefore, we suppose that the high- $T_c$  superconductivity in ultrathin FeSe on MgO is fully controllable by the application of an electric field and confirm that a thickness of one/two unit cells of FeSe itself is not superconducting on MgO, as distinct from on SrTiO<sub>3</sub> substrates.

Finally, we discuss possible mechanisms for the high- $T_c$  superconductivity in FeSe EDL transistors from the view point of

the thickness dependence. The comparable values of  $T_c^{\text{on}}$  shown in Fig. 2c,d for SrTiO<sub>3</sub> and MgO suggest that the electric-field effect induces superconductivity at 40 K despite one possibly expecting different electron–phonon coupling between the FeSe film and the substrate<sup>10</sup>. Concomitantly, the small thickness dependence of  $T_c^{\text{on}}$  below a thickness of ten unit cells indicates that an ultrathin condition, particularly for a single unit cell itself, probably does not play a crucial role in the increase of  $T_c$  for the superconductivity of ultrathin FeSe. Nevertheless, the origin of the difference in the critical thickness for SrTiO<sub>3</sub> (9.6 nm) and MgO (5.9 nm) is still not clear at present, although it may be linked to the degree of charge transfer from the substrates to the FeSe. Naively, it is likely that the positive  $V_G$  depletes holes in the valence band at the  $\Gamma$  point and accumulates electrons in the conduction band at the M point and the interface between the IL and the thick FeSe does not work as the high- $T_c$  superconducting channel (see Fig. 1c). As a consequence, a similar modification of the electronic band structure at the  $\Gamma$  and M points, as proved by ARPES for the single-unit-cell and three-unit-cell FeSe on SrTiO<sub>3</sub> exhibiting large superconducting gap energy<sup>5,29</sup>, may be realized by applying an electric field below the critical thicknesses on SrTiO<sub>3</sub> and MgO. In other words, the electric-field effect in FeSe-EDLT expands the modified layer width yielding the high- $T_c$  superconductivity, which was one/two-unit-cell FeSe in the case of charge doping only from the SrTiO<sub>3</sub> substrate. Furthermore, we suppose that the whole sample contributes high- $T_c$  superconductivity when the modified layer width at IL/FeSe interface touches the interface of the FeSe/substrates. This is what we observed in  $R_s$ - $T$  curve as the single-step transition. However, further investigation into the modification of electronic band structures in etched FeSe under the application of  $V_G$  is required to verify our speculation.

By employing the EDL transistor configuration, high- $T_c$  superconductivity in ultrathin FeSe films has been investigated

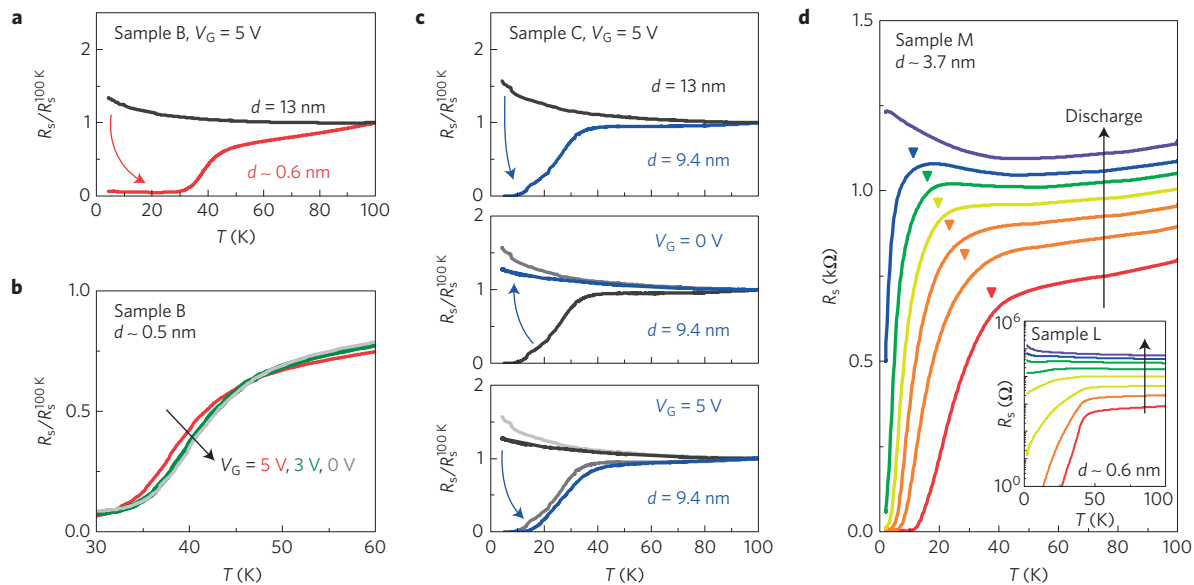


**Figure 3 | Electrostatic tuning of superconductivity.** **a**, Normalized sheet resistance  $R_s/R_s^{100\text{K}}$  as a function of temperature  $T$  for sample B in the initial 13-nm-thick state while applying  $V_G = 5\text{ V}$  (grey solid line) and after etching down to approximately one/two unit cells in thickness with  $V_G = 5\text{ V}$  (red solid line). **b**,  $R_s$ - $T$  data for sample B after thinning to one/two unit cells in thickness.  $V_G$  is reduced from  $V_G = 5\text{ V}$  (red), to  $3\text{ V}$  (green), to  $0\text{ V}$  (grey). **c**, The reversible variation in the  $T$  dependence of  $R_s/R_s^{100\text{K}}$  for sample C against  $V_G$ . (Top panel) The initial insulating (13 nm thick) states with  $V_G = 5\text{ V}$  (grey solid line) and the superconducting behaviour after electrochemical etching to a 9.4-nm-thick condition at  $V_G = 5\text{ V}$  (blue). (Middle panel) Blue solid line shows  $R_s/R_s^{100\text{K}}$  after setting  $V_G$  to  $0\text{ V}$ . (Bottom panel) Blue solid line shows  $R_s/R_s^{100\text{K}}$  with the second application of  $V_G = 5\text{ V}$ . **d**,  $R_s$ - $T$  curves measured for sample M under a 3.7-nm-thick condition. Transition behaviour is presented as a reducing charge from the red solid line (fully charged at  $V_G = 5\text{ V}$ ) to the purple solid line (fully discharged at  $V_G = 0$ ) passing through the other colour lines (partially discharged in turn). Triangles correspond to the values of  $T_c^{\text{on}}$ . Insets: The same experiments carried out on sample L with an approximate thickness of one/two unit cells.

from several perspectives, such as thickness and substrate material dependence. The application of the electric-field effect to induce modification of the electronic band structure would be a major contribution towards  $T_c^{\text{on}}$  values of 40 K below a thickness of ten unit cells regardless of substrate material. Our demonstration of etching that is controlled well by the temperature of the IL under an applied  $V_G$  sheds light on new aspects of the EDL transistor as a useful approach in carrying out ultrathin-film studies and expands the opportunities for demonstrating *ex situ* the superconductivity of ultrathin FeSe grown on various insulating substrates<sup>12,13,15,30</sup>.

## Methods

Methods and any associated references are available in the [online version of the paper](#).

Received 15 April 2015; accepted 24 September 2015;  
published online 2 November 2015

## References

- Kamihara, Y., Watanabe, T., Hirano, M. & Hosono, H. Iron-based layered superconductor  $\text{La}[\text{O}_{1-x}\text{F}_x]\text{FeAs}$  ( $x = 0.05\text{--}0.12$ ) with  $T_c = 26\text{ K}$ . *J. Am. Chem. Soc.* **130**, 3296–3297 (2008).
- Haindl, S. *et al.* Thin film growth of Fe-based superconductors: From fundamental properties to functional devices. A comparative review. *Rep. Prog. Phys.* **77**, 046502 (2014).
- Hsu, F. C. *et al.* Superconductivity in the PbO-type structure  $\alpha\text{-FeSe}$ . *Proc. Natl Acad. Sci. USA* **105**, 14262–14264 (2008).
- Liu, D. *et al.* Electronic origin of high-temperature superconductivity in single-layer FeSe superconductor. *Nature Commun.* **3**, 931 (2012).
- He, S. *et al.* Phase diagram and electronic indication of high-temperature superconductivity at 65 K in single-layer FeSe films. *Nature Mater.* **12**, 605–610 (2013).
- Tan, S. *et al.* Interface-induced superconductivity and strain-dependent spin density waves in FeSe/SrTiO<sub>3</sub> thin films. *Nature Mater.* **12**, 634–640 (2013).
- Peng, R. *et al.* Measurement of an enhanced superconducting phase and a pronounced anisotropy of the energy gap of a strained FeSe single layer in FeSe/Nb:SrTiO<sub>3</sub>/KTaO<sub>3</sub> heterostructures using photoemission spectroscopy. *Phys. Rev. Lett.* **112**, 107001 (2014).
- Peng, R. *et al.* Tuning the band structure and superconductivity in single-layer FeSe by interface engineering. *Nature Commun.* **5**, 5044 (2014).
- Liu, X. *et al.* Dichotomy of the electronic structure and superconductivity between single-layer and double-layer FeSe/SrTiO<sub>3</sub> films. *Nature Commun.* **5**, 5047 (2014).
- Lee, J. J. *et al.* Interfacial mode coupling as the origin of the enhancement of  $T_c$  in FeSe films on SrTiO<sub>3</sub>. *Nature* **515**, 245–248 (2014).
- Wang, Q. Y. *et al.* Interface-induced high-temperature superconductivity in single unit-cell FeSe films on SrTiO<sub>3</sub>. *Chin. Phys. Lett.* **29**, 037402 (2012).
- Sun, Y. *et al.* High temperature superconducting FeSe films on SrTiO<sub>3</sub> substrates. *Sci. Rep.* **4**, 6040 (2014).
- Zhang, W. *et al.* Interface charge doping effects on superconductivity of single-unit-cell FeSe films on SrTiO<sub>3</sub> substrates. *Phys. Rev. B* **89**, 060506(R) (2014).
- Zhang, W. H. *et al.* Direct observation of high-temperature superconductivity in one-unit-cell FeSe films. *Chin. Phys. Lett.* **31**, 017401 (2014).
- Ge, J. F. *et al.* Superconductivity above 100 K in single-layer FeSe films on doped SrTiO<sub>3</sub>. *Nature Mater.* **14**, 285–289 (2015).
- Bozovic, I. & Ahn, C. A new frontier for superconductivity. *Nature Phys.* **10**, 892–895 (2014).
- He, J. F. *et al.* Electronic evidence of an insulator–superconductor crossover in single-layer FeSe/SrTiO<sub>3</sub> films. *Proc. Natl Acad. Sci. USA* **111**, 18501–18506 (2014).
- Ueno, K. *et al.* Field-induced superconductivity in electric double layer transistors. *J. Phys. Soc. Jpn* **83**, 032001 (2014).
- Peck, S. R. *et al.* Response of the double-layer capacitance of a high-temperature superconductor/fluid electrolyte interface to the onset of superconductivity. *J. Am. Chem. Soc.* **114**, 6771–6775 (1992).
- McDevitt, J. T., Riley, D. R. & Haupt, S. G. Electrochemistry of high-temperature superconductors. Challenges and opportunities. *Anal. Chem.* **65**, A535–A545 (1993).
- Haupt, S. G. *et al.* Reversible modulation of superconductivity in YBa<sub>2</sub>Cu<sub>3</sub>O<sub>7- $\delta$</sub> /polypyrrole sandwich structures. *Proc. SPIE* **2158**, 238–249 (1994).
- Bollinger, A. T. *et al.* Superconductor-insulator transition in La<sub>2-x</sub>Sr<sub>x</sub>CuO<sub>4</sub> at the pair quantum resistance. *Nature* **472**, 458–460 (2011).

23. Leng, X., Garcia-Barriocanal, J., Bose, S., Lee, Y. & Goldman, A. M. Electrostatic control of the evolution from a superconducting phase to an insulating phase in ultrathin  $\text{YBa}_2\text{Cu}_3\text{O}_{7-x}$  films. *Phys. Rev. Lett.* **107**, 027001 (2011).
24. Yamada, Y. *et al.* Electrically induced ferromagnetism at room temperature in cobalt-doped titanium dioxide. *Science* **332**, 1065–1067 (2011).
25. Nakano, M. *et al.* Collective bulk carrier delocalization driven by electrostatic surface charge accumulation. *Nature* **487**, 459–462 (2012).
26. Yuan, H. *et al.* Electrostatic and electrochemical nature of liquid-gated electric-double-layer transistors based on oxide semiconductors. *J. Am. Chem. Soc.* **132**, 18402–18407 (2010).
27. Ueno, K., Shimotani, H., Iwasa, Y. & Kawasaki, M. Electrostatic charge accumulation versus electrochemical doping in  $\text{SrTiO}_3$  electric double layer transistors. *Appl. Phys. Lett.* **96**, 252107 (2010).
28. Nojima, T. *et al.* Hole reduction and electron accumulation in  $\text{YBa}_2\text{Cu}_3\text{O}_y$  thin films using an electrochemical technique: Evidence for an *n*-type metallic state. *Phys. Rev. B* **84**, 020502(R) (2011).
29. Miyata, Y., Nakayama, K., Sugawara, K., Sato, T. & Takahashi, T. High-temperature superconductivity in potassium-coated multilayer FeSe thin films. *Nature Mater.* **14**, 775–779 (2015).
30. Bang, J. *et al.* Atomic and electronic structures of single-layer FeSe on  $\text{SrTiO}_3$  (001): The role of oxygen deficiency. *Phys. Rev. B* **87**, 220503(R) (2013).

## Acknowledgements

The authors thank S. Tanaka and T. Ouchi for experimental help and M. Kawasaki, Y. Iwasa and K. Fujiwara for stimulating discussions. This work is partly supported by Grant-in-Aid for Scientific Research on Innovative Areas (No. KAKENHI 22103004) from MEXT of Japan and Grant-in-Aid for Specially Promoted Research (No. KAKENHI 25000003) from the Japan Society for the Promotion of Science (JSPS).

## Author contributions

J.S., T.N. and A.T. conceived and designed this research. Y.I. and J.S. performed thin-film growth and electrical measurements. T.M. and T.N. prepared the electrical measurement system for the EDL transistor device configuration in a liquid helium vessel. Y.I. and J.S. analysed the data and all authors jointly discussed the results. J.S., T.N. and A.T. wrote the manuscript and all authors commented on the manuscript.

## Additional information

Supplementary information is available in the [online version of the paper](#). Reprints and permissions information is available online at [www.nature.com/reprints](http://www.nature.com/reprints). Correspondence and requests for materials should be addressed to J.S.

## Competing financial interests

The authors declare no competing financial interests.

## Methods

**Sample fabrication.** The FeSe films were grown at 300 °C on insulating SrTiO<sub>3</sub>(001) and MgO(001) substrates by pulsed-laser deposition with an as-delivered FeSe target (Kojundo Chemical Laboratory), followed by *in situ* post annealing at 450 °C for 30 min. The growth rate with a laser repetition rate of 5 Hz is approximately 17 nm h<sup>-1</sup>, the value of which is estimated by X-ray Laue fringes (see Supplementary Information). After cutting the film into a 2 × 5 mm<sup>2</sup> rectangular pieces, the channel and the four-terminal electrode (indium pads) were prepared to confine the current flow within the channel by scratching the film. Then, the electrodes were covered with a silicone sealant to prevent them from reacting chemically with the ionic liquid. A platinum plate for the side gate electrode was placed next to the FeSe channel on the same chip and indium pads were attached to the gate electrode in the same way (see Supplementary Information). Then, the FeSe channel and the gate electrode were covered by the ionic liquid, *N,N*-dethyl-*N*-methyl-*N*-(2-methoxyethyl)ammonium bis(trifluoromethanesulphonyl)imide (DEME-TFSI) to form an EDL transistor configuration, as shown in Fig. 1a. To suppress degradation of the sample in air, we carried out the EDL fabrication process as soon as possible. However, it usually

took 6 h before starting the measurement and the sample surface was inevitably exposed to air for about 2–3 h. The thickness after etching is estimated from the initial thickness and the etching rate by summing the leakage current (see Supplementary Information). Surface roughness contributes a ±0.6 nm error to the thickness.

**Electrical measurements.** The sheet resistance  $R_s$  is measured by the standard four-terminal method, where a constant current of typically 0.5 μA is applied and the longitudinal voltage drop is measured by a nanovoltmeter. The temperature is controlled by dipping the sample into the liquid helium vessel in electrical measurements for samples A–C. The sample temperature is monitored by means of a calibrated resistance thermometer (Cernox1050 resistor) inserted in the copper block where the sample is mounted. The  $R_s$ – $T$  curve and magnetotransport properties for samples M and N are measured using a Quantum Design physical property measurement system (PPMS). To control the doping level electrostatically through EDL tuning, we fix the temperature at  $T = 220$  K while varying  $V_G$ . In contrast, the occurrence of the electrochemical reaction is controlled by tuning  $T$  in the range from 240 to 250 K while keeping a constant  $V_G = 5.0$  V.